Nonlocal Energy Deposition in High-Intensity Laser-Plasma Interactions

Jon M. Wallace

Los Alamos National Laboratory, Los Alamos, New Mexico 87545

(Received 2 May 1985)

Electrons heated by the absorption of laser energy on planar targets generate megagauss magnetic field which, together with the coproduced electric fields, transport the electrons away from the laser spot. We present a computational model showing that these superthermal electrons deposit their energy into plasma thermal energy in an expanding annular region in the target plane centered at the spot. The model provides a quantitative explanation for some complex and heretofore poorly understood lateral transport phenomenology.

Recent experiments on lateral transport in high-intensity laser interactions with planar foil targets have shown that a significant fraction of the laser energy deposited in the target is subsequently transported large distances (millimeters) from the laser spot along the target surface prior to conversion to plasma thermal energy.[1-4] The location of electron thermal energy in a target in relation to the laser spot has important implications for laser-driven inertial-confinement fusion, as it is the thermal energy which produces the ablation and resultant implosion of a fusion target. In particular there is the important issue of the drive symmetry[5] provided by a given pattern of laser spots. Consequently, it is essential that mechanisms for nonlocal thermal energy deposition in laser-irradiated targets be well understood.

For a target subjected to high-intensity laser irradiation, superthermal electrons, produced near the critical surface by resonance absorption and some parametric processes, emerge from the laser spot in a plume directed back toward the laser. Recently, particle-in-cell (PIC) computer simulations of the transport of superthermal electrons in a plasma of near-critical density have shown that these electrons can carry a significant amount of energy away from the focal spot.[6] The mechanism is simple: A megagauss magnetic field directed parallel to the target surface is produced with an initial growth rate proportional to $\nabla n_e \times \nabla \theta_e$, where n_e is the hot-electron density and θ_e is the hot-electron temperature. Additionally, the usual outward-normally directed electric field of a thermally expanding plasma is produced.[7] The superthermal electrons ejected from the plasma undergo $\mathbf{E} \times \mathbf{B}$ drift away from the laser spot in the coronal region in front of the target. The PIC simulation showed for the case of 10^{14}-W/cm^2 CO_2-laser irradiation ($\lambda = 10.6$ μm) that some tens of percent of the hot-electron energy deposited into the target could be transported 100-μm distances away from the focal spot on a time scale of tens of picoseconds.[6]

Unfortunately, even the most sophisticated self-consistent plasma simulations cannot be compared directly with experiment. They encompass too small a spatial region over too short a time interval. To do otherwise is impossible with present computer capabilities. We present here a model which treats the larger (millimeter) spatial distances and the longer (100-ps) time scales of the laboratory, bridging the gap between the PIC model and experiment. This is done by giving up the strict field-particle self-consistency of PIC, while imposing close agreement with that model to the extent possible. Our model is the first to produce numerical results for detailed comparison with lateral transport data and, in fact, is in close agreement with the data. The model is essentially a sequence of superthermal-electron trajectory computations in specified electric and magnetic fields.[8] It is directed toward longer-wavelength (≥ 1 μm), high-intensity irradiations, where a significant fraction of the energy deposited on target takes the form of superthermal electrons produced by resonance absorption.

More precisely, electrons sampled from a hot anisotropic half-Maxwellian, with $v_z > 0$, are launched from random locations within a cylindrical laser-deposition region (with radius r_0 and ends z_1, z_2). See Fig. 1. The source region is imagined to be near the critical surface. The electron distribution has a temperature of $\theta_z = 20$ keV in the outward-normal direction and $\theta_r = 2.5$ keV parallel to the target surface. The energy introduced per unit time is held fixed to simulate a constant-intensity laser pulse. The trajectory of each electron in the region in front of the target is computed until the electron intersects the target surface, where the density is substantially supercritical, taken to be the $z = 0$ plane.

The electric field employed is the quasineutral self-similar solution for isothermal expansion of a plasma into a vacuum, $E_z = (\theta_e m_i / Z)^{1/2} / et$, where m_i is the ion mass, e the electron charge, Z the ionization, and t time.[7]

The magnetic field near the laser spot is taken from cylindrical PIC simulations,[9] which showed, for 10-μm irradiation, growth on a 10-ps time scale to a quasisaturated configuration, where the magnetic pressure is

balanced by the plasma pressure. The field here is parametrized according to

$$B_\theta^s \,(r,z) = B_0 \exp\{-\,[(z-z_0)/\Delta z]^2\} \times \begin{cases} r/r_0, & \text{for } r < r_0, \\ r_0/r, & \text{for } r_0 < r < r_1, \end{cases} \tag{1a}$$

where $r_0 < r_1 \sim 100 \ \mu$m.

At larger r, beyond the PIC mesh, where superthermal electrons penetrate the target interior, the r dependence is modified by use of Ampère's law:

$$B_\theta(r,z,t)/B_\theta^s \,(r_1,z) = (r_1/r) \int_0^r J_z(r',t)r'\,dr' \Big/ \int_0^{r_1} J_z(r',t)r'\,dr' \tag{1b}$$

for $r > r_1$, where $J_z(r',t)$ is the hot-electron current density at $z = 0$. The falloff is thus faster than r^{-1} at large r. Equations (1), appropriately rescaled for 1-μm irradiation, are supported by laboratory measurements of the self-generated magnetic field.[10]

The model computation is iterative. The $J_z(r',t)$ obtained from one set of trajectory calculations is used in Eq. (1b) to obtain an improved estimate of the field **B** for use in a successive set of trajectory calculations. The procedure is found to converge rapidly so that no essential changes are obtained after the third iteration. The electric field contains the dominant time dependence in the model, producing even for an r^{-1} static magnetic field the basic features of the hot electron trajectories. (The time dependence of **B** simply gives a more sharply defined deposition annulus.)

The $J_z(r,t)$ given by the model is taken to be a measure of the energy-deposition profile in the target interior and, hence, the x-ray emission, because an elec-

tron penetrates the $z = 0$ surface after it has fallen out of the influence of the magnetic field to be drawn deep into the target by the electric field as a return-current effect.[11] The model parameters are set equal to values near those of the experiments: $r_0 = 70 \ \mu$m, $r_1 = 400 \ \mu$m, $z_0 = 50 \ \mu$m, $\Delta z = 20 \ \mu$m, $z_1 = 34 \ \mu$m, $z_2 = 44 \ \mu$m, $B_0 = 0.8$ MG, $Z = 1$, and $\theta_e = 10$ keV. The electron-deposition profiles for a succession of equally spaced time intervals are shown in Fig. 2. A clearly expanding annular deposition region is indicated by the increasing radius of the second deposition maximum outside the laser spot. There is a decreasing velocity of expansion with time as indicated by the decreasing rate of change of the deposition pattern from the initial velocity of $\sim 10^9$ cm/sec. These features are in strik-
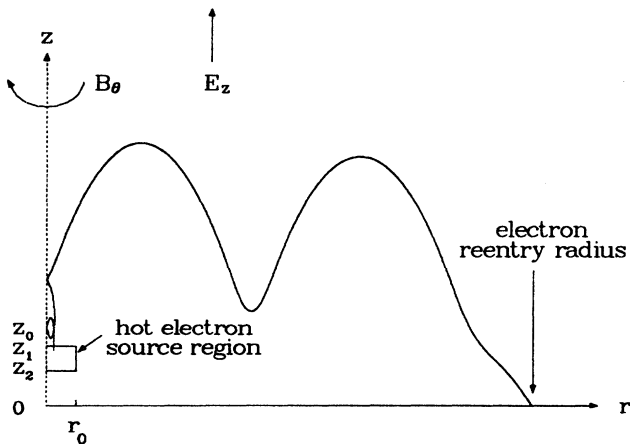
FIG. 1. Schematic diagram of the geometry of the model. The z axis is the cylindrical symmetry axis. The surface of the target where the density is supercritical is taken to be the $z = 0$ plane. The hot-electron source region near critical density is a cylinder with radius r_0 and ends at z_1 and z_2. The directions of the electric and magnetic fields are indicated. A typical computed electron trajectory is shown. (The r dimension has been compressed by a factor of 10 relative to the z dimension.) z_0 is the axial position of maximum B_θ. The apparent reflection of the trajectory off the z axis represents a passage near $r = 0$.
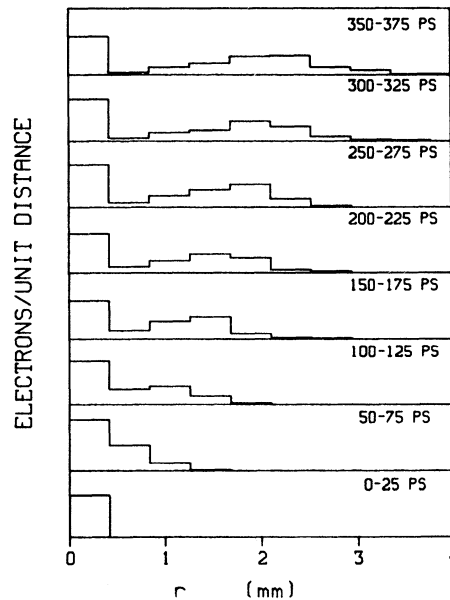
FIG. 2. Electron target deposition profiles for equally spaced 25-ps time intervals. We have plotted the number of electrons reentering the target in each 400-μm-wide annulus during the indicated time interval. The general deposition pattern consists of a large central circular contribution at the laser spot with a second maximum in an expanding annular region. The rate of expansion of the annulus decreases with time from an initial value of $\sim 10^9$ cm/sec.

708
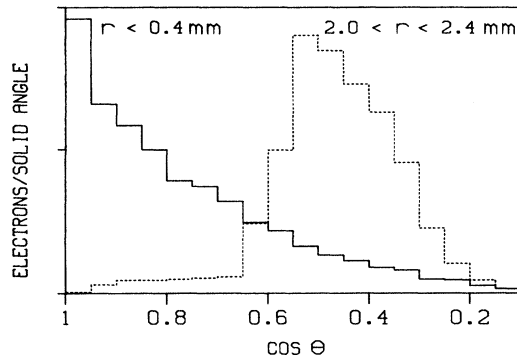
FIG. 3. Normalized time-integrated angular distributions for electrons reentering the target at $r < 0.4$ mm and at $2.0 < r < 2.4$ mm. Time has been integrated over 500 ps starting from $t = 0$. The angle θ is that between the reentrant electron trajectory at $z = 0$ and the inward-directed normal. The solid-line plot for $r < 0.4$ mm shows a predominantly normal angular distribution near the laser spot. The dashed-line plot for $2.0 < r < 2.4$ mm shows penetration well away from the laser spot occurring predominantly at angles greater than 50°.

FIG. 4. Normalized time-integrated energy spectra for electrons reentering the target at $r < 0.4$ mm (solid line) and $2.0 < r < 2.4$ mm (dashed line). Time has been integrated over 500 ps starting from $t = 0$. The spectrum near the laser spot is seen to be significantly harder than the spectrum well away from the spot.

ing agreement with x-ray streak-photograph data for 10-μm laser irradiation[1] with $I \sim 5 \times 10^{14}$ W/cm^2 and 1-μm irradiation[2] with $I \sim 3 \times 10^{15}$ W/cm^2. When we consider the time-averaged angular distribution of electrons entering the target, we find that the electrons penetrating near the laser spot are predominantly normally directed, but with increasing radial distance from the spot the predominant angle of penetration become increasingly oblique. This trend, which is in agreement with the data of Kieffer et al.,[4] is illustrated in Fig. 3 where the normalized time-integrated angular distributions of the model for penetration at $r < 0.4$ mm and at 2.0 mm $< r < 2.4$ mm are plotted.

The time-integrated energy spectrum of electrons entering the target softens with increasing distance from the spot. This result, in agreement with the data of Decoste, Kieffer, and Pepin,[3] is illustrated in Fig. 4 where normalized time-integrated spectra for penetration at $r < 0.4$ mm and 2.0 mm $< r < 2.4$ mm are plotted. The effect arises from the time dependence of the electric field in the model, which acts for a longer period on electrons transported far from the source. Physically the superthermal electrons in the target corona give up energy to fast ions. The softening of energy spectrum with distance from the focal spot is not always the case, however. In Ref. 4 a spectral hardening with distance is reported. This could arise from the fact that the $\mathbf{E} \times \mathbf{B}$ transport mechanism favors electrons with sufficient initial energy to overcome the electric field and reach the region of large $\mathbf{B}$. We found that holding $\mathbf{E}$ constant in the model, thus turning off energy transfer to ions, can cause the large-r spectrum to be harder than the focal-spot spec-

trum. Thus a choice of model parameters, physically reasonable or otherwise, where energy transfer to ions is suppressed relative to the initial-energy selection process could give a spectral hardening at large distances from the laser spot. Further laboratory study of the hot-electron spectrum, with an eye toward identification of the experimental parameters determining spectral modification with r, would be useful, providing a severe test for the model.

In summary, the important expanding deposition pattern observed for laser-irradiated planar targets may be explained with a simple physical picture. Superthermal electrons produced in the laser-target interaction are transported away from the spot by the macroscopic electric and magnetic fields self-consistently generated in front of the target. The time dependence of the deposition is induced by the electric field in our model. It has a much longer time scale than the growth of the magnetic field to its maximum value. This physical picture is in agreement with additional experimental data on the angular distributions and energy spectra of hot electrons entering the target.

The author wishes to thank B. Bezzerides for several helpful and interesting conservations.

[1]P. A. Jaanimagi, N. A. Ebrahim, N. H. Burnett, and C. Joshi, Appl. Phys. Lett. **38**, 734 (1981).

[2]F. Amiranoff et al., J. Phys. D **15**, 2463 (1982).

[3]R. Decoste, J.-C. Kieffer, and H. Pepin, Phys. Rev. Lett. **47**, 35 (1981).

[4]J. C. Kieffer et al., Phys. Rev. Lett. **50**, 1054 (1983).

[5]J. H. Nuckolls, L. Wood, A. Thiessen, and G. Zimmerman, Nature (London) **239**, 193 (1972); J. H. Gardner and S. E. Bodner, Phys. Rev. Lett. **47**, 1137 (1981); M. H. Emery, J. H. Orens, J. H. Gardner, and J. P. Boris, Phys. Rev.

Lett. **48**, 253 (1982); S. E. Bodner, J. Fusion Energy **1**, 221 (1981); Y. Kato et al., Phys. Rev. Lett. **53**, 1057 (1984).

[6]D. W. Forslund and J. U. Brackbill, Phys. Rev. Lett. **48**, 1614 (1982).

[7]J. E. Crow, P. L. Auer, and J. E. Allen, J. Plasma Phys. **14**, 65 (1975); P. Mora and R. Pellat, Phys. Fluids **22**, 2300 (1979).

[8]R. Fabbro and P. Mora, Phys. Lett. **90A**, 48 (1982).

[9]J. M. Wallace, D. W. Forslund, and J. U. Brackbill, Proceedings of the Fourteenth Anomalous Absorption Conference, Charlottesville, Virginia, 1984 (to be published); J. M. Wallace, D. W. Forslund, Bull. Am. Phys. Soc. **29**, 1380 (1984); J. M. Wallace, J. U. Brackbill, and D. W. Forslund, to be published.

[10]A. Raven, O. Willi, and P. T. Rumsby, Phys. Rev. Lett. **41**, 554 (1978); A. Raven et al., Appl. Phys. Lett. **35**, 526 (1979); M. D. J. Burgess, B. Luther-Davies, and K. A. Nugent, to be published.

[11]P. Kolodner and E. Yablonovitch, Phys. Rev. Lett. **43**, 1402 (1979).